Applied Catalysis B: Environmental 179 (2015) 458–467

Contents lists available at ScienceDirect

Applied Catalysis B: Environmental

journal homepage: www.elsevier.com/locate/apcatb

Facile synthesis of CeO_2 hollow structures with controllable morphology by template-engaged etching of Cu_2O and their visible light photocatalytic performance

Siman Fang[a,b], Yongji Xin[b], Lei Ge[a,b,*], Changcun Han[b], Ping Qiu[b], Linen Wu[b]

[a] State Key Laboratory of Heavy Oil Processing, College of Science, China University of Petroleum Beijing, No. 18 Fuxue Rd., Beijing 102249, People's Republic of China

[b] Department of Materials Science and Engineering, College of Science, China University of Petroleum Beijing, No. 18 Fuxue Rd., Beijing 102249, People's Republic of China

ARTICLE INFO

Article history:
Received 30 January 2015
Received in revised form 15 May 2015
Accepted 29 May 2015
Available online 30 May 2015

Keywords:
CeO_2 hollow structure
Template-engaged
Morphology-controlled
Photocatalysis

ABSTRACT

The novel ceria (CeO_2) hollow structures with uniform cubic, polyhedral and sphere shapes were successfully synthesized by template-engaged coordinating etching of shape-controlled Cu_2O crystals. The obtained samples were characterized by X-ray diffraction (XRD), scanning electron microscopy (SEM), transmission electron microcopy (TEM), high resolution of transmission electron microcopy (HRTEM), X-ray photoelectron spectroscopy (XPS), electron spin resonance (ESR) and photoluminescence spectroscopy (PL). The photocatalytic oxygen evolution via water oxidation was investigated for CeO_2 hollow structures with varied shapes under visible light irradiation. The photocatalytic results indicate that polyhedral CeO_2 nanocages show the highest photocatalytic activity, in contrast with spherical CeO_2 hollow structure and cubic CeO_2 hollow structure. The excellent catalytic activity can be attributed to the unique properties of the polyhedral CeO_2 nanocages, including efficient light refection through the inner shells, more active sites for enhancing separation efficiency of charge carriers. It is expected that this study could provide helpful results for designing and exploration of novel hollow structures with tunable photocatalytic performance.

1. Introduction

Semiconductor photocatalytic materials have attracted considerable attention due to their potential application in solving current issues such as global warming, energy conservation and environmental pollution et al. [1–4]. To utilize solar energy in a more efficient way, the design and preparation of visible light-active photocatalysts is highly demanded and thus has attracted intensive efforts in the practical application of such photocatalytic system [5–8]. In the recent decades, various semiconductor photocatalysts such as modified TiO_2 [9–10], multi-metal oxides [11–12], sulfides [13], oxynitrides [14–15], and hetero-structures [16–17] have been successfully developed. These compounds show possibilities in photocatalytic water splitting or pollutant degradation under visible light irradiation.

Hollow micro/nanostructures have been used in myriad applications, such as photonic devices, energy storage, and micro-vessels for drug delivery, nanoscale reactors and photocatalysis [18–20]. Previous studies have demonstrated that transition metal oxides of hollow micro-/nano-structure including TiO_2 [21], ZnO [22], Cu_2O [23], SnO_2 [24] and Fe_3O_4 [25] are promising photocatalysts in organic pollutant degradation and photocatalytic water splitting, owing to their low density, large surface area and high light-harvesting efficiency. Therefore, the design and controllable synthesis of hollow nanostructures have attracted considerable interest in recent years due to their promising properties. The template-assisted method is believed to be good choice in the structurally controlled synthesis of single-component nanostructures and thus has been demonstrated to be a powerful strategy in the controlled synthesis of hollow nanostructures.

Due to the diverse and well-controlled morphologies, including cubes, octahedra, truncated octahedra [26], nanowires [27], nanoplates [28] and appropriate reactivity, Cu_2O nanocrystals have

* Corresponding author at: State Key Laboratory of Heavy Oil Processing, College of Science, China University of Petroleum Beijing, No. 18 Fuxue Road, Beijing 102249, People's Republic of China. Tel.: +86 1089739096; fax.: +86 1089739096.
E-mail address: gelei08@163.com (L. Ge).

http://dx.doi.org/10.1016/j.apcatb.2015.05.051
0926-3373/

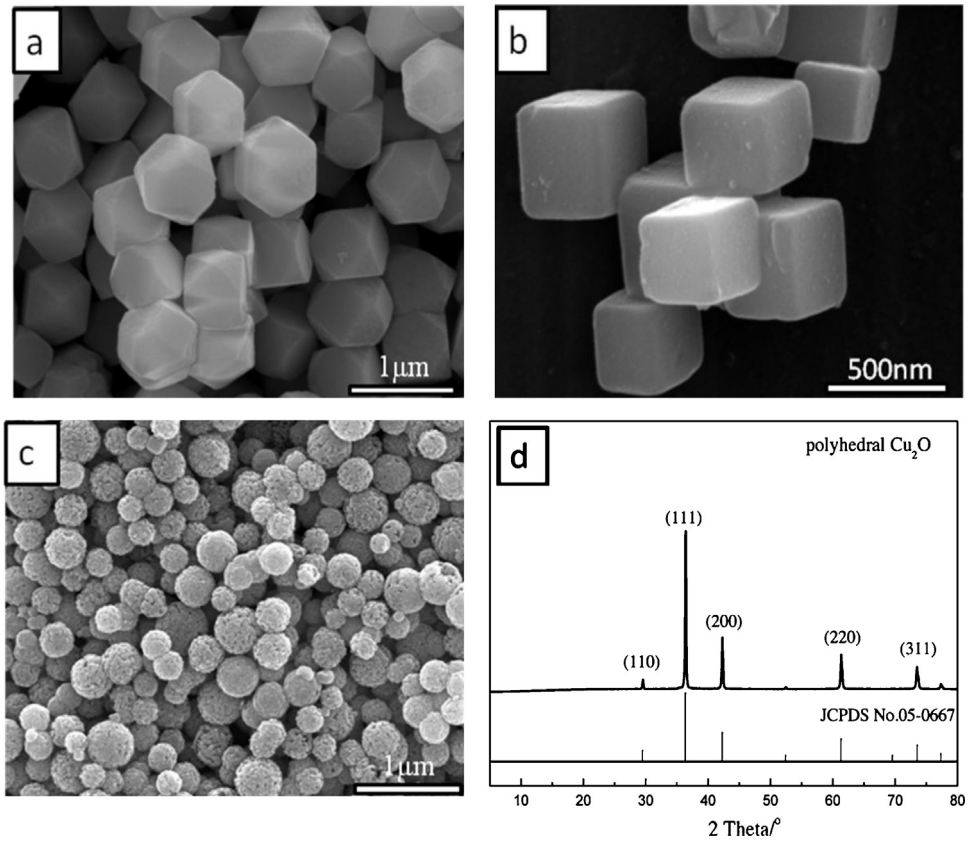

Fig. 1. SEM images of (a) polyhedral; (b) cubic; (c) spherical Cu_2O nanocrystals and (d) XRD patterns of polyhedral Cu_2O nanocrystals.

been much explored as sacrificial templates for the controlled growth of core/shell and hollow nanostructure with various morphologies. Zhang et al. [29] first reported the synthesis of hollow octahedral polyanilline micro/nanostructures by using Cu_2O octahedra as a template in the presence of H_3PO_4. Wang et al. [30] demonstrated the controlled synthesis of various uniform hollow nanostructures including $Fe(OH)_x$ nanocages, SnO_2 nanoboxes, and ZrO_2 nanocages by template-engaged redox etching of shape-controlled Cu_2O nanocrystals. Recently, Nai et al. [31] proposed a general strategy for fabricating uniform nanocages of metal hydroxides (MHs) using Cu_2O nanocrystals as sacrificial templates at room temperature and then obtained metal oxide (MO) nanocages by simple thermal treatment of the as-prepared MHs.

Cerium dioxide (CeO_2), as one of the most important semiconductor materials, is very useful in several key applications, including adsorbents, catalysts, fuel cells, gas sensors, and luminescence [32]. The CeO_2 possesses exceptional catalytic oxidation properties due to its abundant oxygen vacancy defects, high oxygen storage capacity and ability to relatively easily transform between III and IV oxidation states [33]. Despite the success studies, the controlled synthesis of CeO_2 hollow nanostructures for photocatalytic water oxidation has still been limited. Morphology is one of the important factors that determine the performance of the photocatalysts, because different morphologies exhibit different crystal facets, edges and corners, which are considered as active sites in adsorption of reactants [45]. In the present work, we report the preparation of novel CeO_2 hollow nanostructures with controllable morphologies by template-engaged coordinating etching of shape-controlled Cu_2O. The photocatalytic activities of uniform cubic, polyhedral and spherical CeO_2 catalysts were discussed in detail. Simultaneously, possible synthesis and photocatalysis mechanisms were investigated. More importantly, to the best of our knowledge, the research of applying CeO_2 hollow structures as photocatalysts for water splitting reaction is still limited. This study may provide new insight into preparing novel hollow structure materials with potential applications in solar energy conversion and utilization.

2. Experimental

2.1. Materials

Silver nitrate ($AgNO_3$, Aladdin, 99%), sodium hydroxide (NaOH, 99.5%), copper chloride ($CuCl_2{\cdot}2H_2O$, Aladdin, 99%), poly(vinylpyrrolidone) (PVP, Mw = 58000, K29-32, Aladdin, A.R.), ascorbic acid (AA, Aladdin, 99%), sodium thiosulfate ($Na_2S_2O_3$, Aladdin, 99%.), cerium chloride ($CeCl_3{\cdot}7H_2O$, Aladdin, 99.99%), triblock copolymer Pluronic P123($EO_{20}PO_{70}EO_{20}$, Mw = 5800, Energy Chemical), absolute ethyl alcohol (C_2H_6O, A.R.) and ammonia solution ($NH_3{\cdot}H_2O$, 25–28%) were used as received without additional purification or treatment. Milli-Q water was used as the solvent for all of the solutions or dispersions.

2.2. Preparation of CeO_2 hollow nanostructures

Uniform cubic, polyhedral and sphere Cu_2O nanocrystals were synthesized following Zhang's reports with slightly modification [34,35]. To synthesize polyhedral Cu_2O nanocrystals, 10 mL of NaOH aqueous solution (2.0 mol/L) was added dropwise to 100 mL of a $CuCl_2$ aqueous solution (0.01 mol/L) containing 3.33 g of poly(vinylpyrrolidone) (PVP, Mw = 58000) at 55 °C. After the mixture was adequately stirred for 0.5 h, 10 mL of an ascorbic acid aqueous solution (0.6 mol/L) was added dropwise to the solution. The mixed solution was adequately stirred for 3 h at 55 °C. The resulting precipitate was collected by centrifugation, then

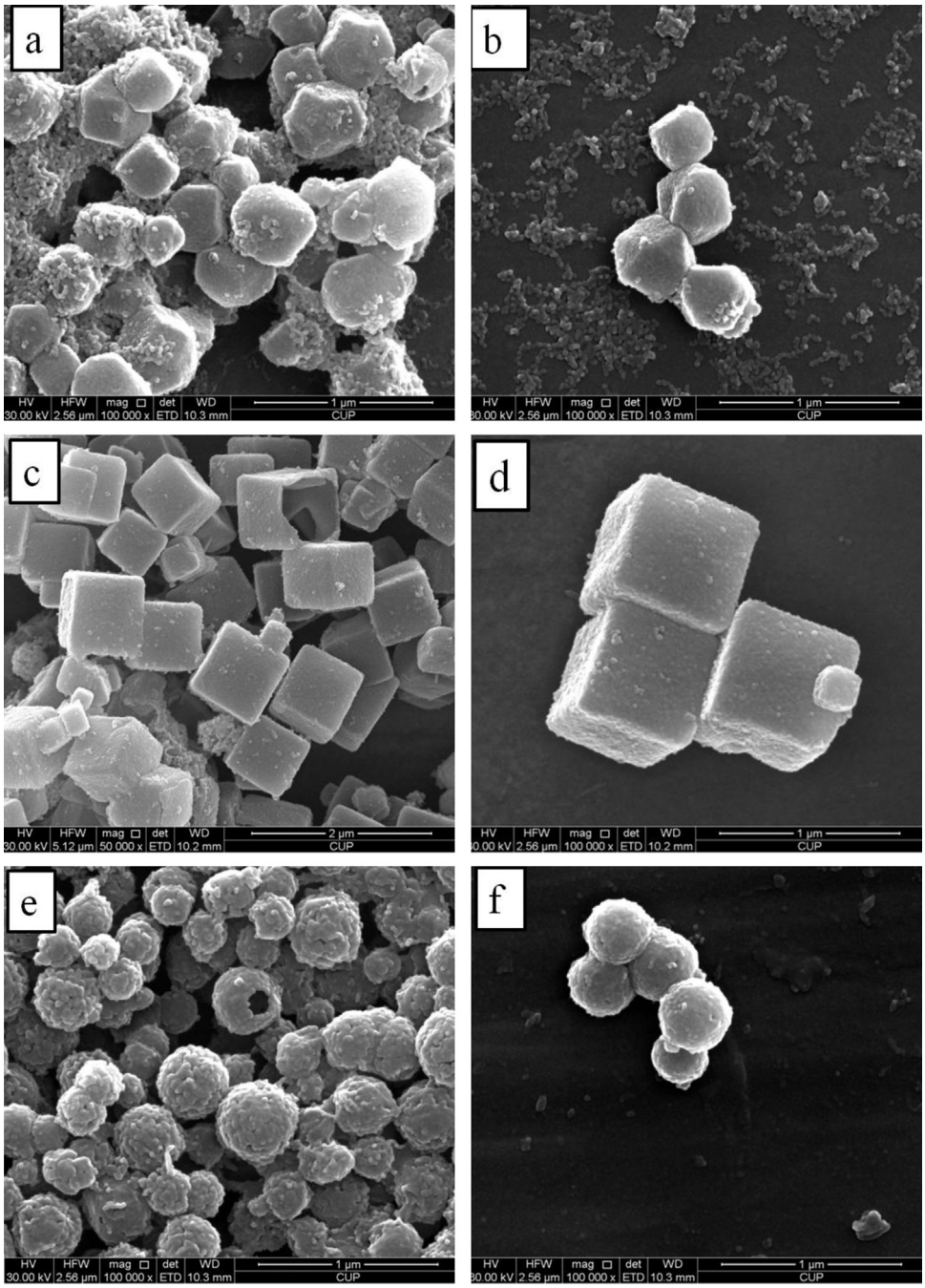

Fig. 2. SEM images of hollow CeO_2 samples with different morphologies: (a) and (b) polyhedron; (c) and (d) cube; (e) and (f) sphere.

washed with distilled water for 3 times and absolute ethanol for twice to remove residual inorganic ions and polymer, and finally dried in vacuum at 60 °C for 6 h. For the synthesis of cubic Cu_2O nanocrystals, all experimental conditions were kept the same as aforementioned except that PVP was not used. To synthesize sphere Cu_2O nanocrystals, 0.612 g triblock copolymer Pluronic P123 was first dissolved in 30 mL deionized water at 18 °C under constant stirring for 3 h. Appropriate volume of ammonia solution ($NH_3{\cdot}H_2O$, 14 M) was added into copper chloride($CuCl_2$, 0.2 M) aqueous solution to keep the molar ratio of NH_3 to Cu^{2+} at 10:1. Then, 2.25 mL $Cu(NH_3)_4{}^{2+}$ solution was poured into the P123 solution under constant stirring. After 30 min, 5.0 mL ascorbic acid (AA, 0.6 M) was added dropwise into the above mixture. All the procedures were kept in water bath at 18 °C. The solution was kept stirring for another 10 min, and the resulting bright yellow precipitate was collected by centrifuging, washing with ethanol for several times to remove the P123 and then drying under vacuum at 60 °C for 6 h.

The CeO_2 hollow structures were synthesized by the template-assisted method employing Cu_2O cubes, polyhedra and spheres as the sacrificial templates. 10 mg of Cu_2O templates and 2.6 mg $CeCl_3{\cdot}7H_2O$ were added to 10 mL of water/ethanol (7:3) mix solvent containing 0.333 g PVP (Mw = 58000). After the mixture was stirred for 10 min, 4 mL, 1 M of $Na_2S_2O_3$ solution was added dropwise. Then the reaction was carried out at room temperature (18–25 °C) for 30 min until the color of suspension change from red to white, and the white precipitate was collected by centrifuging, washing with water and ethanol for three times respectively. Thus, $Ce(OH)_4$ hollow structures were fabricated. Then, the as-prepared $Ce(OH)_4$

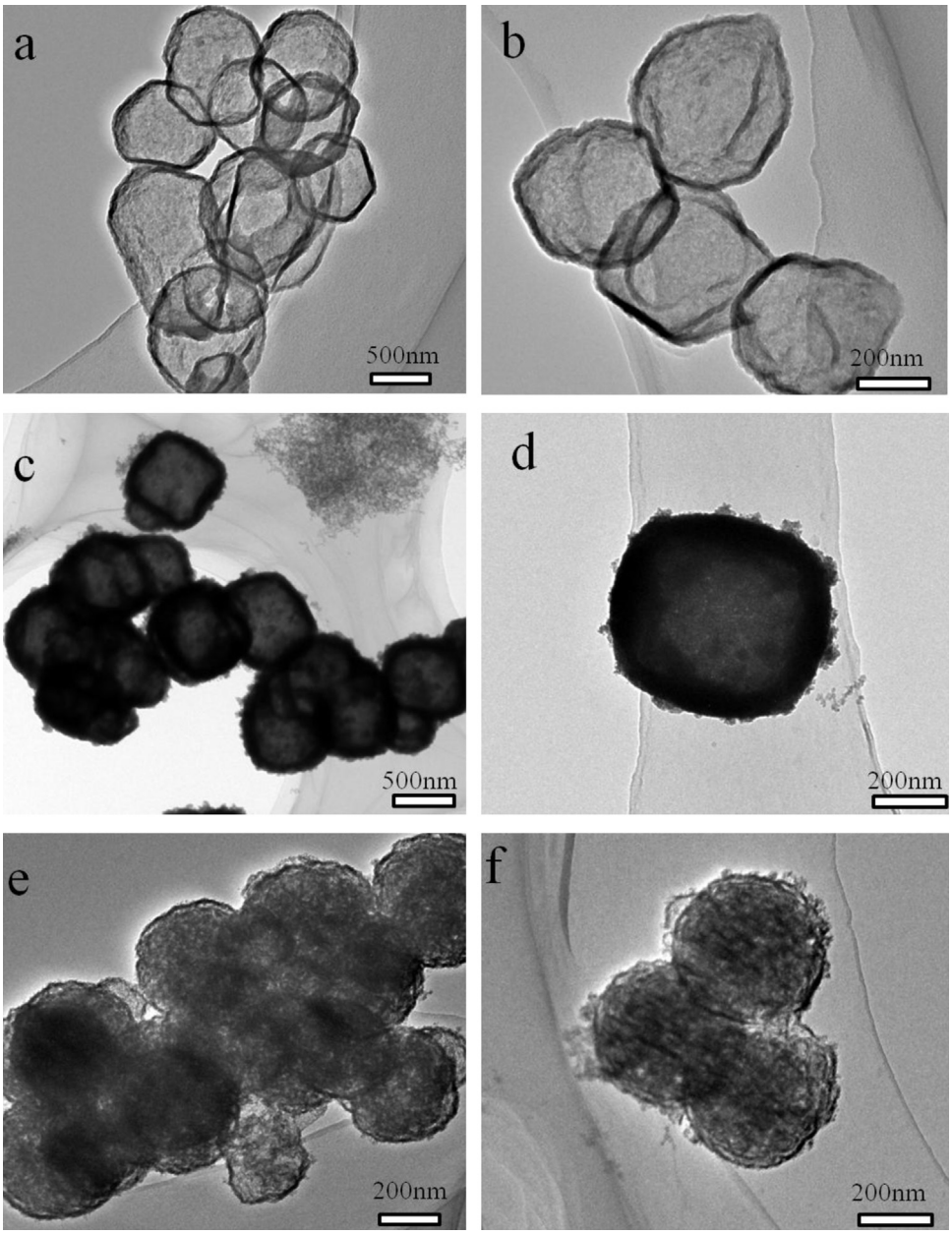

Fig. 3. TEM images of ceria hydroxide ($Ce(OH)_4$) nanocages with different morphology: (a) and (b) polyhedron; (c) and (d) cube; (e) and (f) sphere.

samples were treated with calcinations at 500 °C for 2 h, The heating rate was kept at 1 °C min^{-1}. After heat treatment, CeO_2 hollow structures with different morphologies were obtained. For a comparison, common CeO_2 sample was also prepared under the same experimental conditions without using Cu_2O templates but adjust the pH to 10 with ammonia solution.

2.3. Characterization

The crystal phase of CeO_2 hollow structures were analyzed by X-ray diffraction (XRD; Bruker D8 Advance, X-ray diffractometer) with CuKa radiation at a scan rate of 5 min^{-1}, in the 2θ range of 20–70°. The acceleration voltage and the applied current were 40 kV and 40 mA, respectively. The morphologies of the samples were examined by filed emission scanning electron microscopy (FESEM, FEI Quanta 200F; accelerating voltage = 10 kV) and high-resolution transmission electron microscopy (HRTEM, JEM-2100 and FEI Tecnai G2 F20, accelerating voltage 200 kV). The X-ray photoelectron spectroscopy (XPS) was measured in a PHI 5300 ESCA system. The beam voltage was 3.0 eV, and the energy of Ar ion beam was 1.0 keV. The binding energies were normalized to the signal for adventitious carbon at 284.8 eV. The electron spin resonance (ESR) signals of spin-trapped oxidative radicals were obtained on a Bruker model ESR JES-FA200 spectrometer equipped with a quanta-Ray Nd: YAG laser system as the light source with a UV-cutoff filter ($\lambda \geq 400$ nm). The photoluminescence (PL) spectra of the photocatalyst were obtained by a Varian Cary Eclipse spectrometer with excitation wavelength of 325 nm.

2.4. Evaluation of photocatalytic performance

The photocatalytic O_2 evolution experiments were performed in a 300 mL quartz reactor at 4 °C. The reactor is connected to a low-temperature thermostat bath. PLS-SXE 300UV Xe lamp with a UV-cutoff (≥400 nm) filter was used as the light source. In a typical photocatalytic experiment, 50 mg of photocatalyst powder was

suspended in a 100 mL of aqueous solution containing 0.05 M silver nitrate ($AgNO_3$) solution. Before photocatalytic experiments, the reaction vessel was evacuated for at least 30 min to remove the dissolved air. The products were analyzed by gas chromatography (Beifen 3420A, high purity Argon as a carrier gas, 99.999%) equipped with a thermal conductivity detector.

3. Results and discussion

3.1. Characterization of CeO_2 hollow nanostructures

Fig. 1 presents typical SEM and XRD patterns of the as-synthesized Cu_2O nanocrystal templates. The results indicated that the uniform polyhedral, cubic and sphere Cu_2O with edge length of ~500 nm were successfully synthesized. The XRD patterns in Fig. 1d demonstrates that the structure and component of as-prepared samples can be attributed to Cu_2O phase. All the peaks of polyhedron samples can be readily indexed to the cuprite structure of Cu_2O (JCPDS-No.05-0667). In the preparation process of Cu_2O templates, PVP acted as a capping agent and that preferential adsorbed on the {1 1 1} planes of the Cu_2O crystals and different amount of absorbed PVP can adjust the adsorption kinetic of the surface activities on {1 1 1}, resulting in different growth speed of (1 1 1) and (1 0 0) facets of Cu_2O crystals. Thus, the controllable shapes of Cu_2O can be achieved by adjusting the amount of added PVP, which has been reported in the literature [26].

The as-synthesized Cu_2O polyhedra, cubes and spheres were then employed as sacrificial templates to prepare CeO_2 nanocages via the template-assisted method. The SEM images of typical CeO_2 nanocages with different morphologies are shown in Fig. 2. It can be clearly observed that polyhedral and cubic CeO_2 nanocages were all in length of ~500 nm (Fig. 2a and b) and sphere CeO_2 nanocages were in length of ~300 nm (Fig. 2c), which all inherited the geometrics and dimensions of Cu_2O templates well and no structural deformation such as warping or collapse occurred. The results indicate that the uniform and high quality CeO_2 hollow nanostructures can be prepared by using Cu_2O templating approach.

The hollow interior and architectural construction of as-prepared $Ce(OH)_4$ hollow structures have also been investigated by TEM as displayed in Fig. 3 which illustrates a clear view of these hollow nanostructures. The cagelike $Ce(OH)_4$ samples with the polyhedron, cube and sphere structures, which inherit the geometrics and dimensions of the Cu_2O templates. The inner cavity is clearly revealed by the contrast between the shells and hollow interior. After simple thermal treatment of the as-synthesized $Ce(OH)_4$ samples at 500 °C for 2 h, the relevant CeO_2 nanocages were readily obtained. The crystal structures of CeO_2 hollow structures were investigated by XRD, as shown in Fig. 4. All the diffraction peaks of polyhedron, cube and sphere samples can be ascribed to the fluorite structure of CeO_2 (JCPSD: 81-0792). No additional impurity peaks can be found, implying the high purity of the products.

TEM was used to investigate the microstructure of the CeO_2 hollow structure. Fig. 5 illustrates TEM images of polyhedral, cubic and sphere CeO_2 nanocages. It can be clearly observed from Fig. 5a and b that the CeO_2 nanocages maintain the morphologies and geometries well. Moreover, no obvious structural damage occurs after heat treatment, implying that the present hollow nanostructures can keep stable during the synthesizing process. The CeO_2 shell is composed of small nanoparticles with diameters of about 5 nm (Fig. 5c). And the high-resolution transmission electron microscopy (HRTEM) images further disclose that individual NPs in the shell are highly crystalline with interplanar spacings of 0.312 nm, 0.163 nm and 0.191 nm, corresponding to the (1 1 1), (3 1 1) and (2 2 0) planes of fluorite-type CeO_2, respectively. Fig. 5d is a selected area electron diffraction (SAED) image, indicating the polycrystalline nature of the CeO_2 hollow nanostructures. It is well known that hollow nanostructures can offer large surface areas for catalytic reaction, high dispersion of active sites and enhanced light reflection and absorption in the inner shells [35]. Therefore, the as-prepared CeO_2 hollow structures may have a promising prospect in the applications of photocatalysis and solar energy conversion.

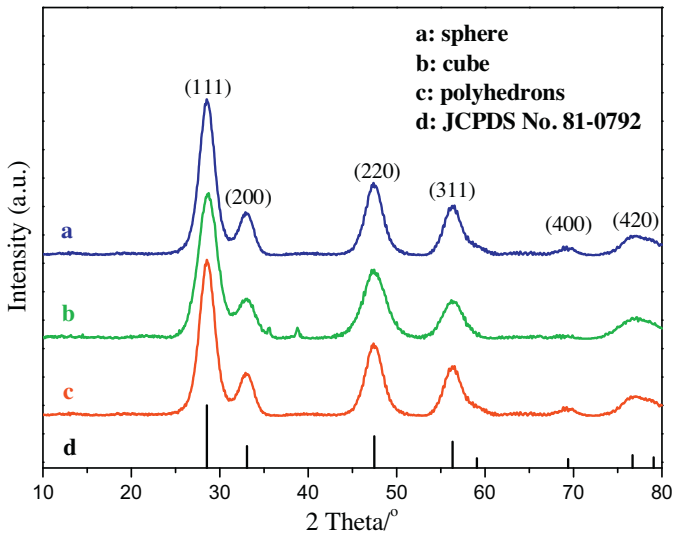

Fig. 4. XRD patterns of hollow CeO_2 samples with different morphologies.

The microscopy results above demonstrate the successful synthesis of CeO_2 hollow structures by the template-assisted method with Cu_2O nanocrystals as the sacrificial templates. The CeO_2 well reproduce the morphology of the employed Cu_2O nanocrystal templates and exhibit hollow nanostructures. These results also supply good examples on demonstrating Cu_2O nanocrystals as versatile sacrificial templates for the fabrication of novel hollow nanostructures.

The elemental composition and chemical status of the CeO_2 hollow structures were further investigated by XPS technique. Fig. 6a–c shows the XPS spectra of the as-prepared polyhedral CeO_2 nanocages. Fig. 6a displays the survey XPS spectrum of the as-prepared CeO_2 nanocages, which mainly contains the peaks of Ce, O, Cu and C. The carbon signal is due to the adventitious hydrocarbon from the XPS instrument itself [39]. The weak copper signal is ascribe to the Cu^+, which remained during the etching reaction and was not washed adequately by distilled water. The sources of the Ce and O peaks correspond to the obtained samples. Fig. 6b shows the XPS spectrum of Ce 3d for polyhedral CeO_2 nanocages. It can be found that the Ce 3d level has a rather complex structure. Six peaks at BEs 882.5, 888.7, 898.2, 900.7, 907.6, and 916.5 (±0.2)eV (marked with a_1, a_2, a_3, b_1, b_2, b_3, respectively) marked with dashed lines due to three pairs of spin-orbit doublets can be attributed to the characteristic of Ce^{4+} 3d final states [36]. The observed peaks can be assigned to CeO_2 (Ce^{4+}) as a_1, a_2 and a_3 for Ce $3d_{5/2}$, with the corresponding Ce $3d_{3/2}$ peaks labeled as b_1, b_2, b_3. Similar spectra have been observed by other literatures for pure CeO_2 [37–38]. It has been demonstrated that the Ce 3d XPS spectrum of a Ce^{4+} compound can be resolved into six structures if some Ce^{3+} species also present, four more structures are presented [40]. Furthermore, CeO_2 and Ce_2O_3 always show peaks at 882.5 and 916.5 eV, as well as at 885 and 903.7 eV, which are considered as being fingerprints characterizing Ce^{4+} and Ce^{3+} oxides, respectively [41]. Consequently, Ce^{4+} is the only oxidation state of the analyzed

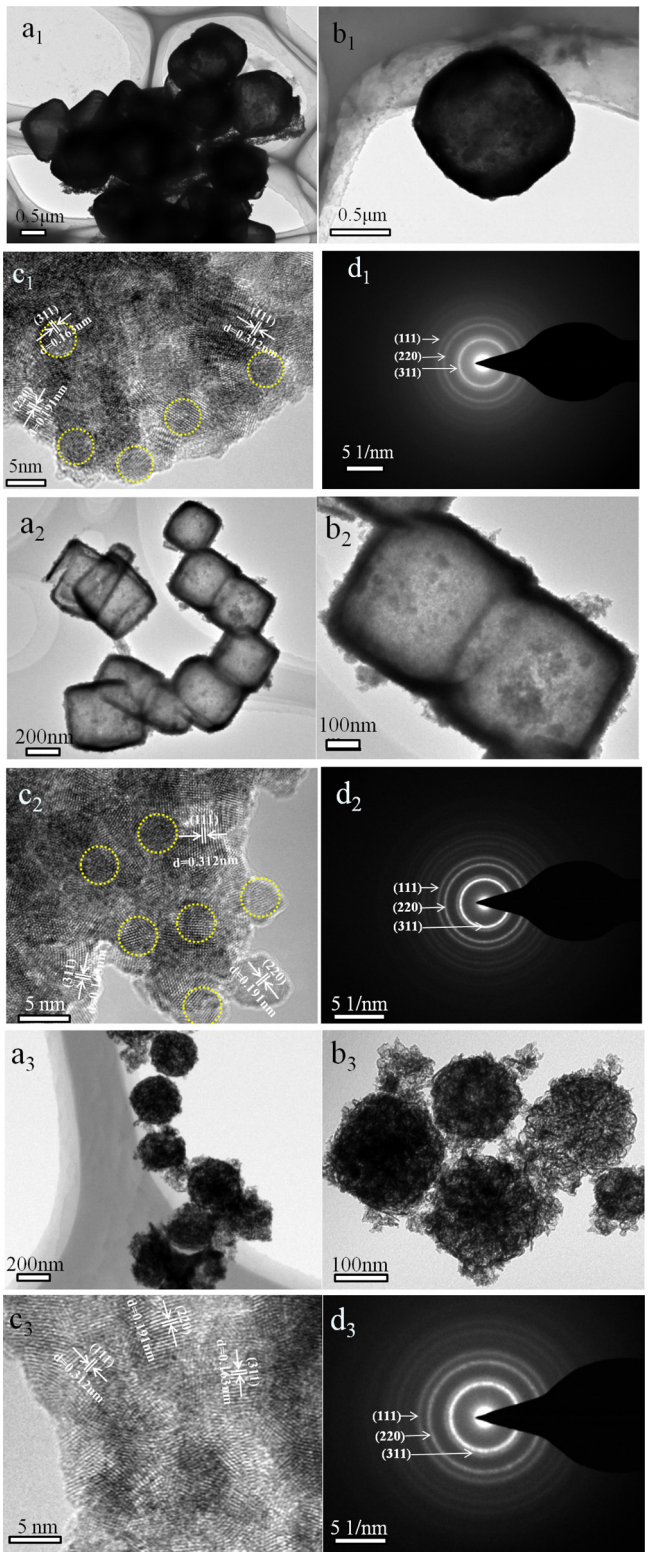

Fig. 5. HRTEM and SAED images of CeO_2 hollow structures: (1) polyhedron; (2) cube; (3) sphere.

CeO_2 polyhedron hollow structures. This result will be confirmed by the study of the O 1s lines showed in Fig. 6c. More information can be also obtained by comparison of the O 1s XPS spectra. It is noticed that the O 1s peak at BE = 529.3 (±0.2 eV), attributed to oxide species, is characteristic of CeO_2 according to Praline et al. [42], who assigned the O 1s peaks at BEs 529.6 and 530.3 eV to CeO_2 and Ce_2O_3, respectively. Whereas the peak at 531.3 eV (BE) is associated with surface adsorbed oxygen such as O^- or OH^- [43]. The XPS results confirm the only presence of Ce^{4+} species on solids surface.

The formation of hollow CeO_2 nanostructures could be qualitatively explained by the template-engaged etching of shape-controlled Cu_2O nanocrystals proposed by Nai et al. [31]. On the basis of the Pearson's hard and soft acid-base (HSAB) principle, on

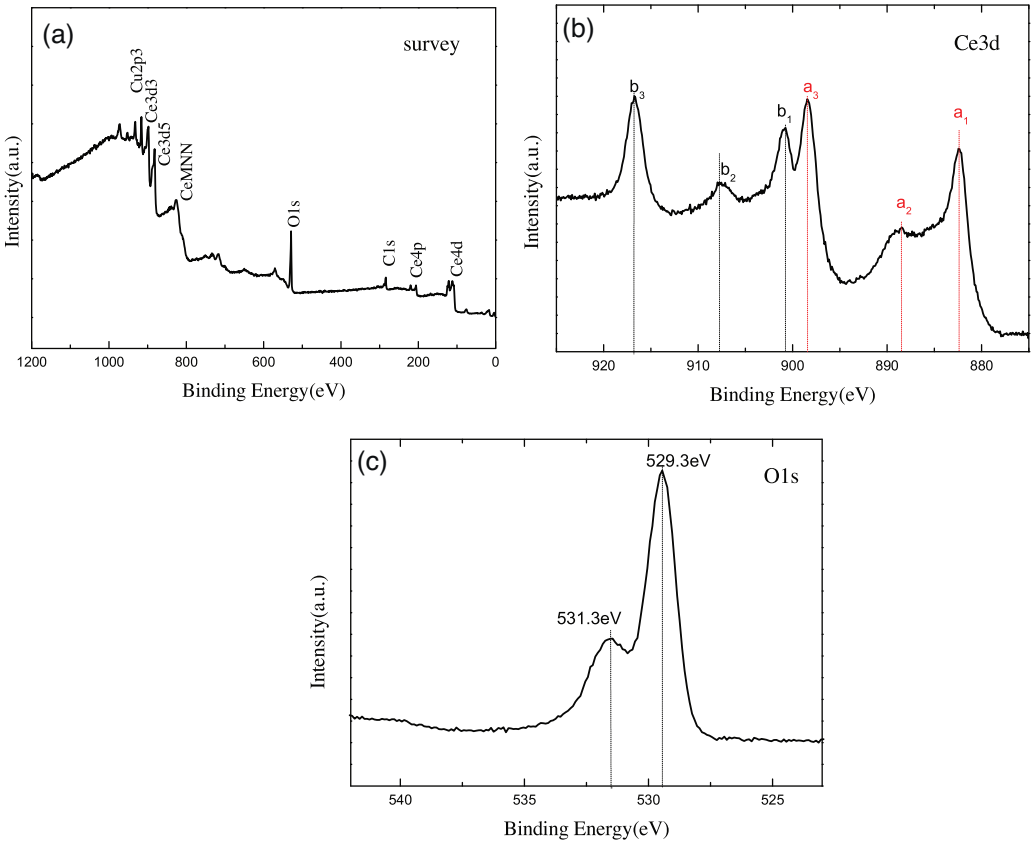

Fig. 6. XPS spectra of the polyhedral CeO_2 hollow structures: (a) survey, (b) Ce3d, (c) O1s.

one hand soft Lewis bases can form stable complexes with soft acids; hard bases, on the other hand, prefer hard acids. Hence, selecting a soft base ligand ($S_2O_3^{2-}$, CN^-, SCN^-, etc.) as the coordinating etchant should be more suitable and efficient than a hard base (Cl^-, NH_3, etc.) due to the soft acid feature of Cu^+ within the Cu_2O templates. In this work, the synthetic strategy of $Ce(OH)_4$ is designed by employing $Na_2S_2O_3$ as the coordinating etchant. The formation process is illustrated as steps 1 and 2 in Fig. 7, and the general chemical route could be described as followed:

$$Cu_2O + xS_2O_3^{2-} + H_2O \rightarrow [Cu(S_2O_3^{2-})_x]^{2-2x} + 2OH^- \quad (1)$$

$$S_2O_3^{2-} + H_2O \rightarrow HS_2O_3^- + OH^- \quad (2)$$

$$Ce^{4+} + 4OH^- \rightarrow Ce_4(OH)_4 \quad (3)$$

$$Ce_4(OH)_4 \rightarrow CeO_2 + 2H_2O \quad (4)$$

During this process, first of all, $S_2O_3^{2-}$ ions are coordinately etching of Cu_2O (Eq. (1)) by emerging a soluble $[Cu(S_2O_3^{2-})_x]^{2-2x}$ species, since the soft–soft interaction of $Cu^+ - S_2O_3^{2-}$ is much stronger than the soft–hard interaction of $Cu^+ - O^{2-}$ within Cu_2O. Secondly, the OH^- produced from the etching of Cu_2O (Eq. (1)), and those coming from hydrolysis of some $S_2O_3^{2-}$ (Eq. (2)) can be used to take part in the formation of $Ce(OH)_4$ (Eq. (3)). Importantly, the pH range of the reaction systems for preparing $Ce(OH)_4$ is alkaline (pH ~10), since much OH^- would be produced when $S_2O_3^{2-}$ etches Cu_2O. Hence, when the etching process starts, $Ce(OH)_4$ begins to precipitate synchronously and the shell structure prefers to form around the etching interface where the local concentration of OH^- is the highest; the process ensures that the outside of $Ce(OH)_4$ shell perfectly inherits the geometrics of Cu_2O templates. Thirdly, as the coordinating etching reaction proceeds, the thickness of the $Ce(OH)_4$ shell would increase until the concentration of Ce^{4+} reduces to a value that cannot meet the demand of precipitating reaction (Eq. (3)). And the dissolution of Cu_2O can continuously occur even in closed shells, proving that species such as $S_2O_3^{2-}$ and the $[Cu(S_2O_3^{2-})_x]^{2-2x}$ species can freely pass through the particle intervals of the shells and are driven by the concentration difference during the etching process (in step 1 and 2). Finally, CeO_2 hollow structures can be readily prepared by the calcinations of the as-prepared $Ce(OH)_4$ samples (Eq. (4)).

From the discussion above, one can perceive that the type of solvent system and the concentration of $CeCl_3$ are crucial for fabricating high-quality $Ce(OH)_4$ nanocages. Excessive water in the solvent system would cause a high concentration of OH^- in the bulk solution by the excessive hydrolysis of $S_2O_3^{2-}$ (Eq. (2)), which would provide more opportunities for some Ce^{4+} to precipitate far from the etching interface and inevitably form abundant irregular particles. While too much ethanol would significantly decrease ionizability and the OH^- concentration, due to the lack of water, leading to only a few formation of $Ce(OH)_4$ nanocages. The concentration of $CeCl_3$ should also be precisely controlled in the system because a much lower concentration of $CeCl_3$ would induce the breakage of nanocages, while a higher concentration of $CeCl_3$ would cause abundant irregular particles, as shown in Fig. 2a and b.

4.1. Visible-light photocatalytic activity of CeO_2 hollow structures

The photocatalytic activities of the hollow CeO_2 samples were evaluated by oxygen evolution in aqueous solutions with silver nitrate as sacrificial reagents under visible light irradiation (>400 nm). Fig. 8 shows the O_2 evolution curves of hollow CeO_2 samples with different morphologies. The curves for O_2 generation indicate that the morphologies of CeO_2 hollow structures have great impact on the catalytic performance.

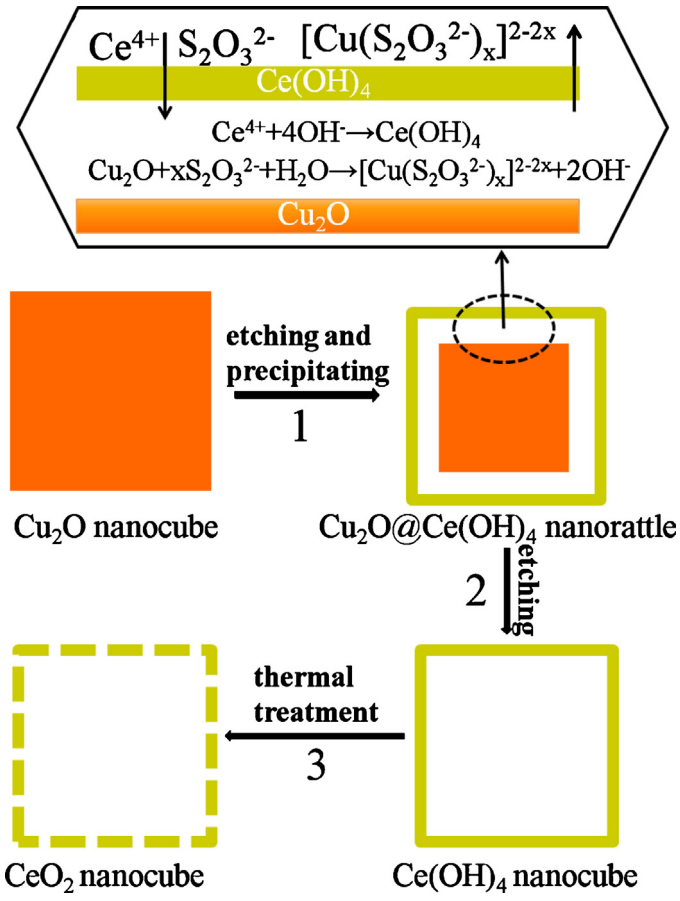

Fig. 7. Schematic illustration of the formation of CeO_2 hollow structures by template-engaged coordinating etching of Cu_2O nanocubes.

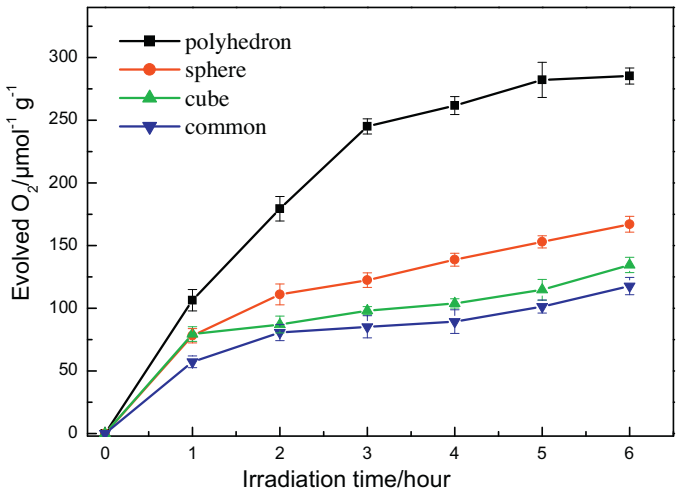

Fig. 8. Photocatalytic O_2 evolution curves of hollow CeO_2 with different morphologies from 0.05 M silver nitrate aqueous solution under visible light illumination ($\lambda \geq 400$ nm). Data points represent the mean ± 95% confidence intervals from three definitive experiments of each sample.

It can be observed clearly that the photocatalytic activity of the polyhedral CeO_2 nanocages is much higher than that of the common CeO_2 nanoparticles, the cubic and spherical CeO_2 nanocages. The average O_2 evolution rates from water oxidation are 22.4 μmol g^{-1} h^{-1} for cubic CeO_2 nanocages, 27.8 μmol g^{-1} h^{-1} for spherical nanocages, 19.6 μmol g^{-1} h^{-1} for common CeO_2 nanoparticles and 47.5 μmol g^{-1} h^{-1} for polyhedral CeO_2 nanocages. Specially, polyhedral CeO_2 nanocages exhibit the highest initial rate, which can reach to 106 μmol g^{-1} at the first hour. The average O_2 evolution rates of hollow CeO_2 structures in our study are higher than the single-shelled and double-shelled CeO_2 hollow microspheres reported in ref [20]. The slope of the O_2 formation curve decreases remarkably even in a short time. This can be attributed to the reason that CeO_2 undergoes fast deactivation with the deposition of Ag particles under present experimental conditions. Such superior activities of polyhedral CeO_2 nanocages may originate from the follow reasons. First, the more exposed facets of CeO_2 polyhedron structure can assist multiple reflections of the incident light, leading to more efficient harvest of the irradiating light and then improved catalytic activity; secondly, the more exposed facets of CeO_2 polyhedron sample can provide larger surface areas and more active sites, which are favorable for both trapping of photoexcited electrons at CB by Ag^+ ions and consumption of holes to release O_2, resulting in efficient separation of excited electron–hole pairs. The results highlight that the unique advantages of CeO_2 hollow structures as water oxidation photocatalysts, giving rise to active sites exposure and superior catalytic activity.

To further investigate the photocatalytic process, the electron spin resonance (ESR) technique was conducted. The electron spin resonance (ESR) technique can be used to detect free radicals in reaction systems. To explain the main reactive species responsible for the photocatalytic reaction over the CeO_2 hollow structure, a series of quenchers were employed to scavenge the relevant reactive species. Typically, DMPO (5, 5-dimethyl-1-dimethy *N*-oxide) generally used as a radical scavenger due to the generation of stable free radical, DMPO—$^{\bullet}O_2^-$ or DMPO—$^{\bullet}$OH. Fig. 9a shows ESR spectra measured as the effect of light irradiation on the polyhedral CeO_2 nanocages at room temperature in air. As shown in Fig. 9a, there was no ESR signal in the dark, a gradual evolution of ESR peaks for DMPO—$^{\bullet}O_2^-$ adducts was observed under visible light irradiation. Fig. 9b illustrates that the DMPO—$^{\bullet}$OH species were clearly observed under light irradiation. Therefore, it is well recognized that in the CeO_2 hollow structures, both superoxide radical ($^{\bullet}O_2^-$) and hydroxyl radical ($^{\bullet}$OH) are produced and play predominant role toward the oxygen evolution reaction under visible light irradiation.

Photoluminescence (PL) measurements were performed to determine the charge recombination and migration behaviors of the CeO_2 hollow structures. Fig. 10 gives the PL spectra of the uniformed cubic, polyhedral and spherical CeO_2 hollow structures at an excitation wavelength of 325 nm. As shown in Fig. 10, the emission intensity of the PL spectrum of the polyhedral CeO_2 nanocages is the lowest in the three morphologies. Lower photoluminescence intensity means a lower electron–hole recombination rate and, hence, a longer lifetime of the photogenerated carriers [44]. Therefore, lower PL spectrum intensity indicates that the polyhedral CeO_2 hollow structures can efficiently prolong the lifetime of photogenerated electron–hole pairs, which is consistent with the photocatalytic experiments.

Based on the results of the structure characterizations and the visible light photocatalytic activities of hollow CeO_2 structures, a possible mechanism for photocatalytic O_2 evolution over hollow CeO_2 catalyst is proposed and illustrated in Fig. 11. Under visible light irradiation, the CeO_2 hollow structure absorbs photons and excites electron–hole pairs. It is clear that the polyhedral CeO_2 hollow structure has better light absorption than the normal solid particles due to multiple reflections within the structure. The excellent light-harvest features can generate more active sites, which are advantageous for production of photo-excited electrons and holes. The photogenerated electrons can react with the oxygen molecules adsorbed on the surface of the CeO_2 photocatalyst to yield $^{\bullet}O_2^-$, while the holes can react with water to yield $^{\bullet}$OH. The as produced superoxide radical anions ($^{\bullet}O_2^-$) and hydroxyl radicals ($^{\bullet}$OH) can

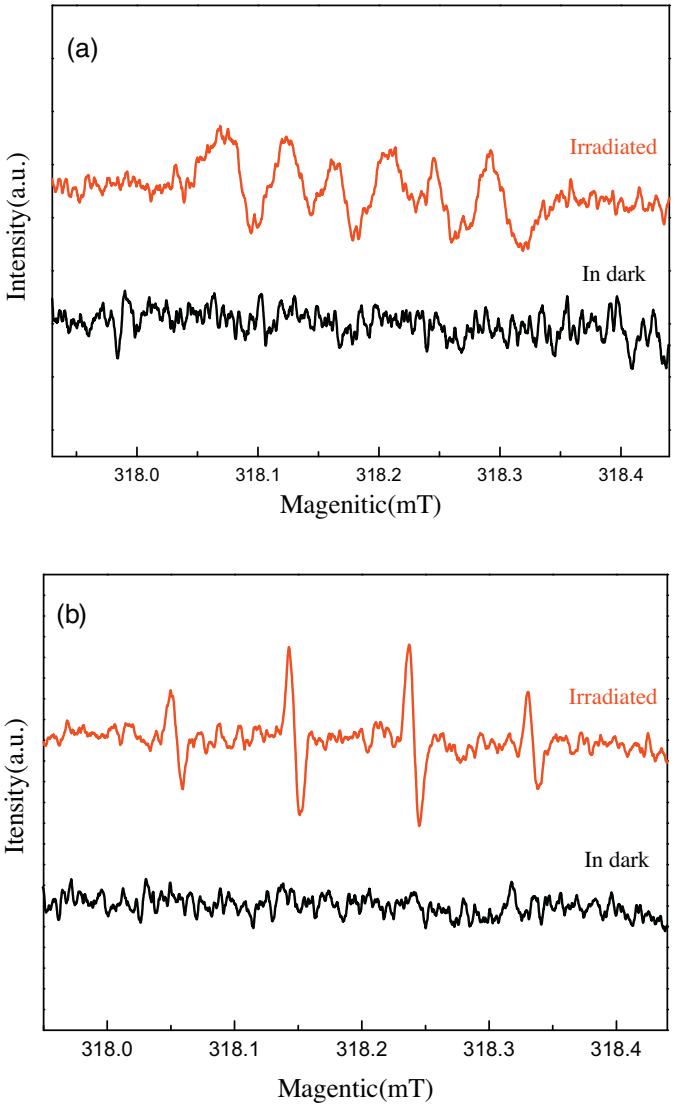

Fig. 9. ESR spectra of radical adducts trapped by DMPO (DMPO—$^{\bullet}O_2^-$) (a); DMPO (DMPO—$^{\bullet}OH$) (b) in the polyhedral CeO_2 nanocages dispersion solution.

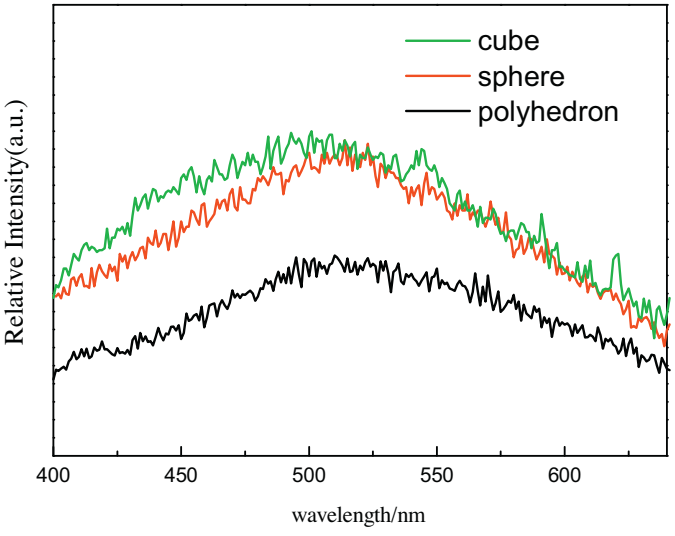

Fig. 10. Photoluminescence spectra (PL) of the cubic, spherical and polyhedral CeO_2 hollow structures.

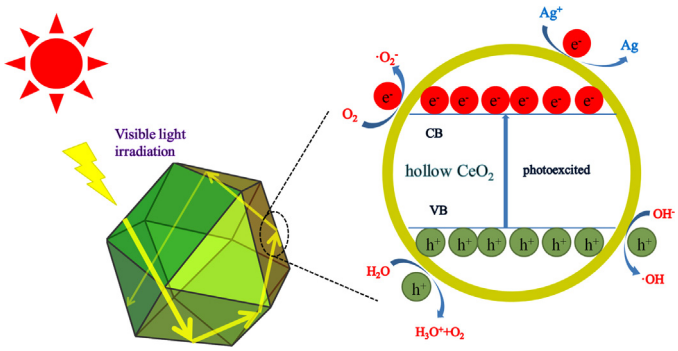

Fig. 11. The schematic illustration for photocatalytic O_2 evolution mechanism over CeO_2 hollow structures under visible light irradiation.

be responsible for the photocatalytic activity of the CeO_2 hollow structures. On the other hand, photogenerated holes can react with water to evolved O_2 directly, whereas the redundant electrons are consumed by the electrons scavenger (Ag^+) in the solution.

5. Conclusions

In summary, we have successfully prepared CeO_2 hollow structures with designed shapes by template-engaged coordinating etching of shape-controlled Cu_2O crystals. Uniformed cubic, polyhedral and spherical hollow CeO_2 nanostructures were obtained by employing corresponding shapes of Cu_2O crystals as templates. The method allows the morphology and dimension of resultant products to be rationally tailored. The obtained CeO_2 hollow structures with cubic, polyhedral and spherical morphologies were polycrystalline phase with fluorite structures and the formation mechanism can be reasonably explained by HSAB principle. The polyhedral CeO_2 nanocages showed the highest photocatalytic activity among the samples with O_2 evolution rate of 47.5 $\mu mol\, h^{-1}\, g^{-1}$. This possibly depends on the higher surface area and more active sites for adsorption of reactants and improving separation of electron–hole pairs. Therefore, it is expected that these CeO_2 hollow nanostructures obtained via sample preparing methods can provide promising potentials for new energy applications.

Acknowledgements

This work was financially supported by the National Science Foundation of China (Grant No. 21003157 and 21273285), Beijing Nova Program (Grant No. 2008B76), and Science Foundation of China University of Petroleum, Beijing (Grant No. KYJJ2012-06-20).

Appendix A. Supplementary data

Supplementary data associated with this article can be found, in the online version, at http://dx.doi.org/10.1016/j.apcatb.2015.05.051

References

[1] A. Fujishima, K. Honda, Nature 238 (1972) 37–38.
[2] X. Chen, H.Y. Zhu, J.C. Zhao, Z.F. Zheng, X.P. Gao, Angew. Chem. 120 (2008) 5433–5436.
[3] G. Liu, Y. Zhao, C. Sun, F. Li, G.Q. Lu, H.M. Cheng, Angew. Chem. Int. Ed. 47 (2008) 4516–4520.
[4] Y.G. Su, Y.N. Xia, Science 298 (2002) 2176–2179.
[5] G. Wang, B.B. Hang, X.C. Ma, Z.Y. Wang, X.Y. Qin, X.Y. Zhang, Y. Dai, M.H. Wang, Angew. Chem. 52 (2013) 4810–4813.
[6] Y.J. Xin, L.E. Wu, L. Ge, C.C. Han, Y.J. Li, S.M. Fang, J. Mater. Chem. A 3 (2015) 8659–8666.
[7] Z. Yang, D. Han, D. Ma, H. Liang, L. Li, Y. Yang, Cryst. Growth Des. 10 (2009) 291–295.

[8] C.C. Han, L.E. Wu, L. Ge, Y.J. Li, Z. Zhao, Carbon 92 (2015) 31–40.
[9] J.G. Yu, G.P. Dai, Q.J. Xiang, M. Jaroniec, J. Mater. Chem. 21 (2011) 1049–1057.
[10] X.B. Chen, L. Liu, P.Y. Yu, S.S. Mao, Science 331 (2011) 746–750.
[11] J.W. Tang, Z.G. Zou, J.H. Ye, Angew. Chem. Int. Ed. 43 (2004) 4463–4470.
[12] X.G. Kong, Z.L. Guo, P.H. Wen, L.Y. Cao, J.F. Huang, C.Y. Li, J. Fei, F. Wang, Q. Feng, RSC Adv. 4 (2014) 56637–56644.
[13] C.C. Hu, Y.L. Lee, H.S. Teng, J. Phys. Chem. C 115 (2011) 2805–2811.
[14] K. Maeda, K. Domen, MRS Bull. 36 (2011) 25–31.
[15] K. Maeda, M. Hiqashi, D.L. Lu, R. Abe, K. Domen, J. Am. Chem. Soc. 132 (2010) 5858–5868.
[16] L. Kong, Z. Jiang, T.C. Xiao, L.F. Lu, M.O. Jones, P.P. Edwards, Chem. Commun. 47 (2011) 5512–5514.
[17] H.J. Huang, D.Z. Li, Q. Lin, Y. Shao, W. Chen, Y. Hu, Y.B. Chen, X.Z. Fu, J. Phys. Chem. C 113 (2009) 14264–14269.
[18] X.W. Lou, L.A. Archer, Z.C. Yang, Adv. Mater. 20 (2008) 3987–4019.
[19] Y.D. Yin, R.M. Rioux, C.K. Erdonmez, S. Hughes, G.A. Somorjai, A.P. Alivisatos, Science 304 (2004) 711–715.
[20] J. Qi, K. Zhao, G.B. Li, Y. Gao, H.J. Zhao, R.B. Yu, Z.Y. Tang, Nanoscale 6 (2014) 4072–4077.
[21] X. Wu, G.Q. Lu, L. Wang, Energy Environ. Sci. 4 (2011) 3565–3572.
[22] X. Wang, M. Liao, Y. Zhong, J.Y. Zheng, W. Tian, T. Zhai, C. Zhi, Y. Ma, J. Yao, Y. Bando, D. Golberg, Adv. Mater. 24 (2012) 3421–3425.
[23] H. Xu, W. Wang, Angew. Chem. Int. Ed. 46 (2007) 1489–1492.
[24] H.X. Yang, J.F. Qian, Z.X. Chen, X.P. Ai, Y.L. Cao, J. Phys. Chem. C 111 (2007) 14067–14071.
[25] B. Wang, H.B. Wu, L. Zhang, X.W. Lou, Angew. Chem. Int. Ed. 52 (2013) 4165–4168.
[26] D.F. Zhang, H. Zhang, L. Guo, K. Zheng, X.D. Han, Z. Zhang, J. Mater. Chem. 19 (2009) 5220–5225.
[27] X. Hong, G. Wang, W. Zhu, X. Shen, Y. Wang, J. Phys. Chem. C 113 (2009) 14172–14175.
[28] C.H.B. Ng, W.Y. Fan, J. Phys. Chem. B 110 (2006) 20801–20807.
[29] Z. Zhang, J. Sui, L. Zhang, M. Wan, Y. Wei, L. Yu, Adv. Mater. 17 (2005) 2854–2857.
[30] Z. Wang, D. Luan, C.M. Li, J. Am. Chem. Soc. 132 (2010) 16271–16277.
[31] J.W. Nai, Y. Tian, X. Guan, L. Guo, J. Am. Chem. Soc. 135 (2013) 16082–16091.
[32] C. Sun, H. Li, H. Chen, Energy. Environ. Sci. 5 (2012) 8475–8505.
[33] N. Zhang, X. Fu, Y.J. Xu, J. Mater. Chem. 21 (2011) 8152–8158.
[34] Y. Shang, D. Zhang, L. Guo, J. Mater. Chem. 22 (2012) 856–861.
[35] X. Li, J.G. Yu, J.X. Low, Y.P. Fang, J. Xiao, X.B. Chen, J. Mater. Chem. A 3 (2015) 2485–2534.
[36] X.W. Liu, K.B. Zhou, L. Wang, B.Y. Wang, Y.D. Li, J. Am. Chem. Soc. 131 (2009) 3140–3141.
[37] E. Abi-aad, R. Bechara, J. Grimblot, A. Aboukais, Chem. Mater. 5 (1993) 793–797.
[38] P. Bera, K.R. Priolkar, A. Gayen, P.R. Sarode, M.S. Hegde, S. Emura, R. Kumashiro, V. Jayaram, G.N. Subbanna, Chem. Mater. 15 (2003) 2049–2060.
[39] M. Kozlowski, Fuel 83 (2004) 259–265.
[40] A. Kotani, T. Jo, J.C. Parlebas, Adv. Phys. 37 (1988) 37–85.
[41] G.M. Ingo, R.D. Maschio, L. Scoppio, Surf. Interface Anal. 18 (1992) 661–666.
[42] G. Praline, B.E. Koel, R.L. Hance, J. Electron Spectrosc. 21 (1980) 17–30.
[43] Z.M. Liu, J.M. Hao, L.X. Fu, T.L. Zhu, Appl. Catal. B 44 (2003) 355–370.
[44] L.Q. Jing, Y.C. Qu, B.Q. Wang, Sol. Energy Mater. Sol. Cells 90 (2006) 1773–1787.
[45] K.B. Zhou, Y.D. Li, Angew. Chem. Int. Ed. 51 (2012) 602–613.